THE JOURNAL OF BIOLOGICAL CHEMISTRY
Vol. 280, No. 5, Issue of February 4, pp. 3555–3563, 2005
Printed in U.S.A.

Structural and Mechanistic Analysis of Sialic Acid Synthase NeuB from *Neisseria meningitidis* in Complex with Mn^{2+}, Phosphoenolpyruvate, and *N*-Acetylmannosaminitol*

Received for publication, October 21, 2004, and in revised form, October 27, 2004
Published, JBC Papers in Press, October 29, 2004, DOI 10.1074/jbc.M411942200

Jason Gunawan‡, Dave Simard§, Michel Gilbert¶, Andrew L. Lovering‡, Warren W. Wakarchuk¶, Martin E. Tanner§‖, and Natalie C. J. Strynadka‡**

From the ‡Department of Biochemistry and Molecular Biology, University of British Columbia, Vancouver, British Columbia V6T 1Z3, §Department of Chemistry, University of British Columbia, Vancouver, British Columbia V6T 1Z1, and ¶Institute for Biological Science, National Research Council of Canada, Ottawa, Ontario K1A 0R6, Canada

In *Neisseria meningitidis* and related bacterial pathogens, sialic acids play critical roles in mammalian cell immunity evasion and are synthesized by a conserved enzymatic pathway that includes sialic acid synthase (NeuB, SiaC, or SynC). NeuB catalyzes the condensation of phosphoenolpyruvate (PEP) and *N*-acetylmannosamine, directly forming *N*-acetylneuraminic acid (or sialic acid). In this paper we report the development of a coupled assay to monitor NeuB reaction kinetics and an ^{18}O-labeling study that demonstrates the synthase operates via a C—O bond cleavage mechanism. We also report the first structure of a sialic acid synthase, that of NeuB, revealing a unique domain-swapped homodimer architecture consisting of a $(\beta/\alpha)_8$ barrel (TIM barrel)-type fold at the N-terminal end and a domain with high sequence identity and structural similarity to the ice binding type III antifreeze proteins at the C-terminal end of the enzyme. We have determined the structures of NeuB in the malate-bound form and with bound PEP and the substrate analog *N*-acetylmannosaminitol to 1.9 and 2.2 Å resolution, respectively. Typical of other TIM barrel proteins, the active site of NeuB is located in a cavity at the C-terminal end of the barrel; however, the positioning of the swapped antifreeze-like domain from the adjacent monomer provides key residues for hydrogen bonding with substrates in the active site of NeuB, a structural feature that leads to distinct modes of substrate binding from other PEP-utilizing enzymes that lack an analogous antifreeze-like domain. Our observation of a direct interaction between a highly ordered manganese and the *N*-acetylmannosaminitol in the NeuB active site also suggests an essential role for the ion as an electrophilic catalyst that activates the *N*-acetylmannosamine carbonyl to the addition of PEP.

Sialic acids are a family of high carbon sugars that play a vital role in a variety of biological functions, such as development, recognition, and cell adhesion. Their prevalence is widespread as they are observed in viruses, mammalian cells, and select microbial organisms (1, 2). These nine carbon 3-deoxy-2-keto sugars are found as a series of repeating units on the termini of secreted and cell surface glycoproteins and glycolipids on bacterial organisms (2). Several species of pathogenic bacteria, such as *Escherichia coli* and *Neisseria meningitidis*, produce sialylated capsular polysaccharides to avert host defenses as they are frequently encountered on the surface of human cells, thereby leading to poor antibody responses (3). In addition, sialylated polysaccharides block targets such as galactose residues on glycoproteins, commonly recognized by innate immunity responses (2, 4). The effect of sialic acid on human morbidity also extends to a variety of cancers, as metastasis and tumorigenesis have been linked to changes in the amount, linkage, and type of sialic acid residues (5, 6). Because of the biological prevalence of sialic acids and, consequently, their attractiveness as potential drug targets, there lies an important need to characterize the complete pathway of their formation. A variety of pathways involved in the synthesis and degradation of sialic acids in bacteria and eukaryotes has been identified; however, little is known about the structural and mechanistic properties of the enzymes involved.

N. meningitidis, a causative agent of meningitis, encodes a sialic acid synthase, NeuB (SiaC, SynC) that directly converts phosphoenolpyruvate (PEP)[1] and *N*-acetylmannosamine (ManNAc) into *N*-acetylneuraminic acid (NeuNAc, or sialic acid) (Fig. 1) (7). Orthologous NeuB enzymes that catalyze the same reaction have been found in other pathogenic organisms such as *E. coli* (8, 9) and *Campylobacter jejuni* (10, 11). The formation of sialic acids in vertebrates occurs in a similar fashion except that NeuNAc 9-phosphate is formed through the condensation of PEP and *N*-acetylmannosamine 6-phosphate by NeuNAc 9-phosphate synthase. The phosphate group is then removed through the action of NeuNAc 9-phosphatase, forming sialic acid (12). The remaining steps in the utilization of sialic acid are similar in both eukaryotes and microbial organisms; CMP-NeuNAc synthetase activates NeuNAc through the addition of CTP, forming CMP-NeuNAc (7), which then becomes the

* This work was funded by awards from the Howard Hughes Medical Institute, Canadian Institute of Health Research, and Canadian Bacterial Diseases Network (to N. C. J. S.), Natural Sciences and Engineering Research Council of Canada (to M. E. T.), and the Michael Smith Foundation for Health Research (to J. G.). The costs of publication of this article were defrayed in part by the payment of page charges. This article must therefore be hereby marked "*advertisement*" in accordance with 18 U.S.C. Section 1734 solely to indicate this fact.

The atomic coordinates and structure factors (codes 1XUU (malate-bound NeuB structure) and 1XUZ (PEP and rManNAc-bound NeuB structure)) have been deposited in the Protein Data Bank, Research Collaboratory for Structural Bioinformatics, Rutgers University, New Brunswick, NJ (http://www.rcsb.org/).

‖ To whom correspondence may be addressed. Tel.: 604-822-9453; Fax: 604-822-2847; E-mail: mtanner@chem.ubc.ca.

** To whom correspondence may be addressed. Tel.: 604-822-0789; Fax: 604-822-5227; E-mail: natalie@byron.biochem.ubc.ca.

[1] The abbreviations used are: PEP, phosphoenolpyruvate; TIM, triose-phosphate isomerase; ManNAc, *N*-acetylmannosamine; rManNAc, reduced ManNAc or *N*-acetylmannosaminitol; ALS, advanced light source; NeuNAc, *N*-acetylneuraminic acid; KDO8PS, 2-keto-3-deoxy-D-*manno*-octulosonate-8-phosphate synthase; DAH7PS, and 2-keto-3-deoxy-D-*arabino*-heptulosonate-7-phosphate synthase; AFP, antifreeze protein.

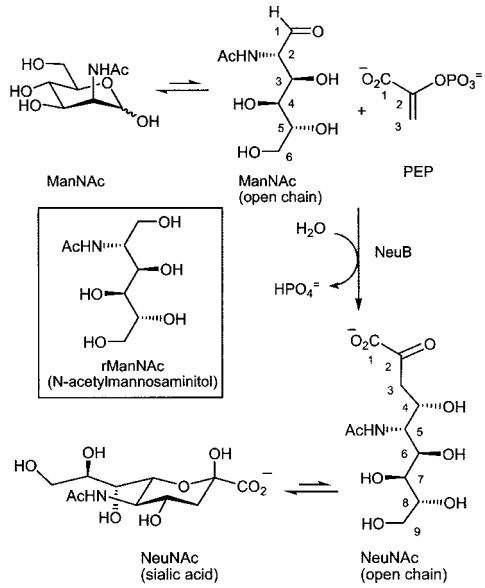

FIG. 1. **Reaction catalyzed by *N. meningitidis* sialic acid synthase (NeuB).** NeuB catalyzes the condensation of PEP with ManNAc creating sialic acid and orthophosphate. The *inset* shows the structure of reduced ManNAc (rManNAc or *N*-acetylmannosaminitol).

substrate for sialyl transferases for addition to the cell surface (13, 14).

Two enzymes, 2-keto-3-deoxy-D-*manno*-octulosonate-8-phosphate synthase (KDO8PS) and 2-keto-3-deoxy-D-*arabino*-heptulosonate-7-phosphate synthase (DAH7PS), are also known to utilize PEP to form complex sugar molecules. KDO8PS catalyzes the condensation of PEP with D-arabinose-5-phosphate to form KDO8P (15), whereas DAH7PS catalyzes the reaction between PEP and D-erythrose-4-phosphate to form DAH7P (16). Extensive information regarding the structural and mechanistic properties of KDO8PS (17–19) and DAH7PS (20–22) is available. A 2.2-Å resolution crystal structure of *T. maritima* DAH7PS in complex with PEP, Cd^{2+}, and D-erythrose 4-phosphate was recently solved; however, the sugar substrate was observed in an apparently non-productive orientation (21). Both KDO8PS and DAH7PS exist as a homotetramer, with each monomer exhibiting an eight-stranded parallel β-barrel fold surrounded by eight helices ($(\beta/\alpha)_8$ barrel) (17, 23), a structure exemplified in triose-phosphate isomerase (TIM) (24). Because very little information regarding the structure or mechanism of sialic acid synthase has been available and given the very low sequence identity with the characterized DAH7PS and KDO8PS (<10% identity for the *E. coli* enzymes), it was not clear if the sialic acid-metabolizing enzymes would adopt a similar fold and active site architecture. In addition, previous studies have shown that the C-terminal region of mammalian sialic acid synthase shares ~40% sequence identity with fish type III antifreeze protein (AFP) (25). These studies suggested that there are likely notable differences between the structure and mechanism of sialic acid synthase and other 2-keto-acid synthases as well as a curious and novel relationship with type III AFPs.

Two general mechanisms may be invoked for the action of sialic acid synthase; one employing C—O bond cleavage and the other employing P—O bond cleavage. Precedence from studies on KDO8PS and DAH7PS would favor the former, in which the C-3 carbon of PEP adds to the carbonyl of ManNAc and water adds to the C-2 position of PEP to give a tetrahedral intermediate (Fig. 2) (18–21, 26–29). This would likely occur in a stepwise fashion involving an oxocarbenium ion intermediate. The tetrahedral intermediate would then lose phosphate to give the open chain form of NeuNAc that would spontaneously cyclize to the pyranose form in solution. A key experiment performed on the KDO8PS and DAH7PS reactions demonstrated that when [2-^{18}O]PEP was used as a substrate, the ^{18}O label was found exclusively in the recovered orthophosphate (30, 31). This is only consistent with a C—O bond cleavage mechanism (see the labeled atoms in Fig. 2). Despite this precedence, chemical intuition may lead one to favor a P—O cleavage mechanism in which water attacks the phosphate of PEP and liberates the enolate anion of pyruvate (not shown). The enolate then adds to the aldehyde of ManNAc to give the open chain form of Neu5Ac. In this case, the use of [2-^{18}O]PEP would lead to label residing in the product and the formation of unlabeled orthophosphate. Similar nucleophilic attacks at the phosphate of PEP are thought to occur with the enzymes pyruvate kinase (32) and PEP carboxykinase (33). The carbon-carbon bond-forming step of such a reaction would resemble that catalyzed by *N*-acetylneuraminic acid lyase, a type I aldolase that catalyzes the reversible cleavage of NeuNAc into pyruvate and ManNAc (34).

To further understand the mechanism of sialic acid synthesis, we report here the first crystal structures of *N. meningitidis* NeuB bound to malate and metal ion co-factor Mn^{2+} and also in complex with reduced ManNAc (*N*-acetylmannosaminitol or rManNAc) (Fig. 1) and PEP. The observed oligomerization state and structural fold define NeuB as unique among the family of PEP-utilizing enzymes. We also report a new assay for the enzymatic activity of the synthase as well as an ^{18}O-labeling experiment that demonstrates sialic acid synthase operates via a C—O bond cleavage mechanism (Fig. 2).

EXPERIMENTAL PROCEDURES

Cloning, Overexpression, and Purification of Untagged Enzyme—Cloning of NeuB, encoded from the *neuB* gene of *N. meningitidis* serogroup B (35), was carried out into the pCWori+ vector, transformed into *E. coli* strain AD202, and grown at 37 °C in 2 liters of Luria-Bertani (LB) medium supplemented with 100 μg ml^{-1} ampicillin. Overexpression of NeuB was induced through the addition of 0.5 mM isopropyl-β-D-thiogalactopyranoside at an A_{600} of ~0.60, with overnight growth at 20 °C. Cells were harvested through centrifugation, washed in 20 mM Tris HCl (pH 8.5), 150 mM NaCl, and lysed with three passes through a French press. The lysate was centrifuged at 40,000 × *g* for 35 min, passed through a 0.45-μm filter, and loaded directly onto a 20-ml bed volume Q-Sepharose column (Amersham Biosciences) equilibrated with 20 mM Tris HCl (pH 8.5), 100 mM NaCl. The column was initially washed with 2× column volume of 20 mM Tris HCl, 100 mM NaCl, then eluted with 1.5× column volume gradient of 100 mM NaCl to 1 M NaCl in 20 mM Tris HCl (pH 8.5). Fractions containing active enzyme were then pooled, and ammonium sulfate was added to a final concentration of 1 M and adjusted to a pH of 7.0. The protein solution was then loaded onto a 100-ml bed volume phenyl-Sepharose column (Amersham Biosciences) equilibrated with 50 mM sodium phosphate (pH 7.0), 1 M ammonium sulfate and eluted with a 1× column volume gradient from 50 mM sodium phosphate (pH 7.0), 1 M ammonium sulfate to 50 mM sodium phosphate (pH 7.0). Fractions containing NeuB were then pooled and dialyzed overnight against 20 mM Tris HCl (pH 8.5), 100 mM NaCl buffer. The dialyzed protein solution was pressure-concentrated by ultrafiltration and purified by a Mono Q anion exchanger (Amersham Biosciences) using a linear gradient of 100 mM NaCl to 1 M NaCl in 20 mM Tris-HCl buffer (pH 8.5). Samples containing eluted protein were then pooled and further dialyzed overnight in 20 mM Tris-HCl (pH 8.5), 100 mM NaCl buffer, pressure-concentrated by ultrafiltration and applied to a Superdex-200 gel filtration column (Amersham Biosciences). Purified protein was concentrated to ~15 mg ml^{-1} for crystallization trials. Selenomethionyl NeuB was prepared as described previously (36) and purified in a similar manner as native NeuB protein.

Cloning, Overexpression, Purification, and Activity Verification of His-tagged Enzyme—The *neuB* gene was cloned into a pET-30 Xa/LIC vector using the Xia/LIC cloning kit protocol (Novagen). The resulting plasmid was transformed into *E. coli* strain JM109 (DE3) expression cells that were grown at 37 °C in 500 ml of LB media containing 30 μg/ml kanamycin. Overexpression of His-tagged NeuB was induced through the addition of 0.5 mM isopropyl-β-D-thiogalactopyranoside at an A_{600} of ~0.60 and grown for an additional 4 h. Cells were harvested

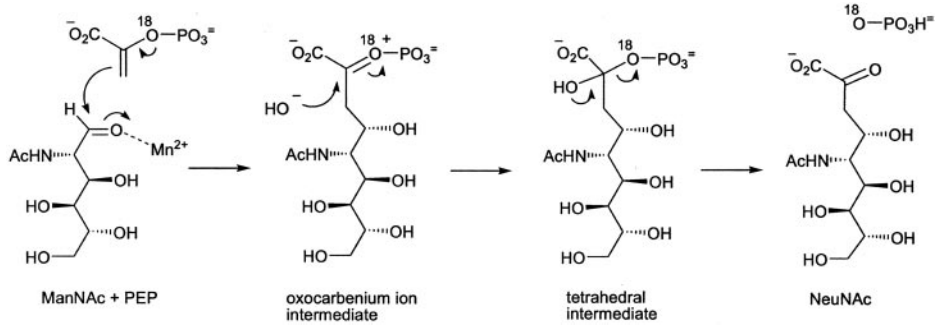

FIG. 2. **The proposed C—O bond cleavage mechanism for the reaction catalyzed by sialic acid synthase (NeuB).** ^{18}O isotopic labels are included to highlight the fate of the bridging phosphate oxygen of PEP during catalysis.

through centrifugation, resuspended in 30 mM triethanolamine-HCl buffer (pH 7.5) (containing 10% glycerol, 1 μg/liter aprotinin and pepstatin, 1 mM phenylmethylsulfonyl fluoride), and lysed with three passes through a French press. The crude protein was loaded onto a chelating Sepharose nickel affinity column (10 ml (pH 8.0); Amersham Biosciences) according to the manufacturer's instructions. The column was washed with 10 and 50 mM concentrations of imidazole, and the protein was eluted with 500 mM imidazole. Fractions containing the enzyme were dialyzed overnight in 30 mM triethanolamine-HCl buffer (pH 7.5) with 1 mM dithiothreitol and 10% glycerol and then flash-frozen. Protein samples were >90% pure as determined by SDS-PAGE analysis. ^{1}H and ^{31}P NMR spectroscopy was used to monitor the purified His-tagged enzymatic reaction and confirmed that the reaction products were NeuNAc and phosphate, respectively. The unmodified enzyme and the His-tagged enzyme showed similar activities, indicating that the presence of the N-terminal modification did not dramatically affect the reaction rate. No reaction could be observed in the presence of 5 mM EDTA, confirming that the divalent cation was vital for activity.

Preparation of rManNAc—Sodium borohydride (0.08 g, 2.0 mmol) was added to a solution of ManNAc (0.21 g, 1.0 mmol) in water (10 ml), and the mixture was stirred at room temperature for 2 h. The solution was neutralized using Amberlite IRP-64 ion exchange resin, filtered, and lyophilized. The white solid was refluxed in methanol (50 ml) for 30 min and then concentrated under reduced pressure. The oily film was dissolved in water and lyophilized to give a white solid (0.16 g).

Crystallization and Data Collection—Purified untagged NeuB at a concentration of 15 mg ml^{-1} and in the presence of 10 mM $MnCl_2$ and a variety of substrates (10 mM reduced ManNAc/PEP/NeuNAc) was used for hanging drop vapor diffusion crystallization trials. Orthorhombic crystals (0.4–0.5 mm) in the space group $P2_12_12$ were obtained using 1.75 M malic acid (pH 6.2) as the precipitant. However, due to the use of high concentrations of malic acid as the precipitant for crystallization, the NeuB active site contained bound malate coordinating the metal co-factor (malate having some chemical similarity to PEP). To remove the malate from the active site, NeuB crystals were soaked in 2 M sodium phosphate (pH 6.2), 10 mM $MnCl_2$, 10 mM PEP, and 10 mM reduced ManNAc for 24 h to facilitate buffer exchange. Crystals were then soaked in 20% (v/v) ethylene glycol (acting as the cryoprotectant), substrate, and metal for 5 min before data collection at 100 K. Single wavelength native (malate-bound) and selenomethionyl data sets were collected at the advanced light source (ALS) beamline 8.2.1 using an ADSC Quantum Q210 CCD detector. Data sets of the NeuB and substrate complexes were collected using a MAR345 detector on a rotating anode Rigaku RU200 generator. The malate-bound $P2_12_12$ NeuB crystal has unit cell dimensions a = 58.8, b = 76.2, c = 77.5 Å, with one molecule per asymmetric unit. The complexed NeuB plus Mn^{2+} plus reduced ManNAc and PEP crystal has unit cell dimensions a = 58.5, b = 75.6, c = 77.9 Å. Malate-bound data were processed using DENZO and SCALEPACK (37), and NeuB complex data were processed using MOSFLM (38) and the CCP4 program suite (39). Data collection and processing statistics are summarized in Table I.

Structure Determination and Refinement—The structure of NeuB was determined through the collection of anomalous diffraction of a highly redundant single wavelength (SAD) data set from orthorhombic crystals grown using selenomethionyl incorporated protein. A total of 8 of a possible 10 selenium atom sites were identified using SnB Version 2.2 (40), with additional site refinement carried out using SOLVE (41) and SHARP (42). Electron density maps were improved via solvent flattening using RESOLVE (43). The initial model was built manually using XTALVIEW (44), and the final model containing all 349 residues in thermodynamically favorable positions was obtained through several rounds of refinement with CNS Version 1.1 (45) to a resolution of 1.9 Å. Bound rManNAc and PEP were modeled at full occupancy as was the Mn^{2+}co-factor. Quality of the model was analyzed with PROCHECK (46), with 93% of residues in the most favorable regions of the Ramachandran plot and no residues in the disallowed region. Figs. 1 and 2 were created with ChemDraw Ultra 8.0 (CambridgeSoft), Figs. 3, 4, 6, and 7 were created with MOLSCRIPT (47). Figs. 3, 4, 6, and 7 were rendered with Raster3D (48).

Static Light Scattering—Static light scattering experiments were carried out at 25 °C on a Superdex 200 gel filtration column using 20 mM Tris-HCl (pH 8.5), 100 mM NaCl. Refractive index and Mini-dawn light scattering detectors (Wyatt Technology) were calibrated using bovine serum albumin (Sigma).

Coupled Assay—A cuvette containing Tris-acetic acid (pH 8.3) (150 mM, 0.8 ml final volume), ManNAc (variable), NADH (160 μM), lactate dehydrogenase (250 units), NeuNAc lyase (20 units, Jülich Fine Chemicals), $MnCl_2$ (1 mM), and dithiothreitol (1 mM) was incubated for 10 min at 37 °C. After the initial incubation, PEP (variable) was added, and the observed slow background rate of PEP hydrolysis was determined by the decrease in absorbance at 340 nm. The enzymatic reaction was initiated by the addition of His-tagged NeuB (1 μg), and the enzymatic rate was calculated from the observed rate less the background rate. The K_m value for ManNAc was measured in the presence of 1 mM PEP, and that for PEP was measured in the presence of 30 mM ManNAc.

^{18}O-Labeling Experiment—[2-^{18}O]PEP disodium salt was prepared using slight modifications to literature-reported procedures (49, 50). The resulting material was 66% enriched in ^{18}O isotope at the C-2 position as determined by both ^{31}P NMR spectroscopy and mass spectrometry. The time 0 reaction mixture contained [2-^{18}O]PEP (5 mg), ManNAc (2.5 mM), dithiothreitol (1 mM), $MgCl_2$ (1 mM), triethanolamine-HCl (pH 7.5) (final concentration of 12 mM in a total volume of 600 μl), and D_2O (200 μl). A proton-decoupled ^{31}P NMR spectrum was obtained with the sweep bandwidth limited to 20 ppm. The synthase (0.3 mg) was added, and the reaction was monitored for 2 h with spectra taken every 30 min.

RESULTS AND DISCUSSION

Subunit Architecture—Each monomer of *N. meningitidis* NeuB consists of 349 residues and can be divided into two distinct domains that are joined by an extended linker region (Fig. 3*b*). The first domain, consisting of residues 1–273, has a fold typical of a TIM barrel (24); that is, an eight-stranded parallel β-barrel enclosed by eight helices (H1-H8). Two additional small α-helices are present between H2 and H3 of the $(\beta/\alpha)_8$ barrel and form part of an extended loop region of NeuB consisting of residues 61–87. Despite low sequence identity (<10%), superposition of the secondary structural elements of the first N-terminal 273 residues of NeuB with other PEP utilizing enzymes such as DAH7PS supports the hypothesis that the enzymes are composed of a very similar overall fold (root mean square deviation value of 2.1 Å on 273 C-α residues).

The second domain of sialic acid synthase is entirely novel for a PEP utilizing enzyme and consists of 74 residues from the C-terminal end of the enzyme, with a linker region consisting of residues 274 to 284 joining it to the N-terminal TIM barrel domain. Residues 285 to 349 form an antifreeze-like domain, similar to that observed in a variety of functional type III AFPs (51, 52). This compact, "pretzel-shaped" fold consists of two identical motifs comprised of four short β-strands and a single 3_{10} helix. The two motifs are arranged with approximate 2-fold

TABLE I
Data collection, SAD phasing, and model refinement statistics

	Malate-bound	Derivative (selenomethionyl) peak	Complex
Data collection			
Space group	$P2_12_12$	$P2_12_12$	$P2_12_12$
Beamline	8.2.1	8.2.1	
Resolution (Å)	1.9	2.7	2.2
Wavelength (Å)	1.5418	0.9796	1.5418
Total reflections	90,130	153,926	69,090
Unique reflections	26,239	12,456	17,331
Redundancy	3.4	12.4	4.0
Completeness (%)[a]	94.0 (69.2)	100.0 (100.0)	98.6 (95.0)
$\langle I/_\sigma(I)\rangle$[a]	6.2 (2.9)	5.9 (1.3)	16.4 (9.2)
R_{sym}[a,b]	7.3 (24.0)	10.7 (57.6)	3.6 (7.8)
Refinement statistics			
Resolution (Å)	30–1.9		30–2.2
Number of atoms			
Protein	2,681		2,681
Substrate	9		25
Water	182		255
R_{cryst} (%)[c]	0.207		0.186
R_{free} (%)[c]	0.238		0.248
Root mean square deviations			
Bonds (Å)	0.005		0.006
Angles (°)	1.3		1.3
Average B-factor (Å^2)			
Protein	25.0		15.9
Substrate	31.4 (malate)		16.2 (PEP) 25.1 (rManNAc)
Water	30.1		21.4

[a] Values in parentheses refer to the highest resolution bin (malate-bound, 2.0–1.9 Å; selenomethionyl, 2.8–2.7 Å; complex: 2.3–2.2 Å).
[b] $R_{sym} = \Sigma|(I_{hkl}) - \langle I\rangle|/\Sigma(I_{hkl})$, where I_{hkl} is the integrated intensity of a given reflection.
[c] $R_{cryst} = (\Sigma|F_o - F_c|)/(\Sigma F_o)$, where F_o and F_c are observed and calculated structure factors.

symmetry, such that the eight total strands of the domain form three small antiparallel β-sheets (two three-stranded and one two-stranded). An eleven residue loop, containing a small 3_{10} helix connects the two motifs together. Superposition of the C-terminal 64 residues from NeuB with other type III AFPs (65 residues total protein length) yields a very highly correlated structural alignment (root mean square deviation of 1.0 Å on the 64 common C-α residues).

Oligomerization State—Previous circular dichroism and matrix-assisted laser desorption ionization time-of-flight spectrometry studies of *E. coli* NeuB had suggested that the enzyme exists as a tetramer in solution, an oligomerization state also observed for both KDO8PS and DAH7PS (53). However, based on the results of our biophysical analysis, we conclude that *N. meningitidis* NeuB preferentially forms a domain-swapped homodimer (Fig. 3*a*) and not a tetramer. Our static light scattering experiments of purified NeuB resulted in the elution of a 78,000-Da peak (data not shown), indicating the presence of a physiological dimer in solution (monomer size is 38,347 Da). The x-ray structure also reveals two antiparallel monomeric NeuB polypeptide chains that are intimately associated across the crystallographic dyad axis, with the linker region between the two domains of a single NeuB monomer, providing an extended groove upon which the TIM barrel domain of the second NeuB chain sits. The total buried surface area of the homodimer is extensive (2393 Å^2), in keeping with a physiologically relevant homodimer. This domain-swapped dimerization allows for three major areas of interactions in the NeuB homodimer. The first interaction involves the close packing of the C-terminal ends of two opposing TIM barrels, the second involves the packing of the linker region of one monomer with an opposing TIM barrel, and finally, the third major region of interaction in the NeuB homodimer lies in the packing of the N-terminal region of the antifreeze-like domain of one monomer with the TIM barrel of the second monomer. It is important to note that at the TIM barrel-antifreeze-like domain interface, the side chains of three residues from the antifreeze-like domain, Thr-285′, Phe-288′, and Arg-314′, are positioned directly within the depressed cavity of the adjacent TIM barrel, where they play a direct role in substrate binding (Fig. 3*c*).

Sialic acid synthases and fish type III AFP have no obvious functional similarities. However, previous studies have shown high sequence identity between the C-terminal end of NeuB and type III AFPs (25). The structure of NeuB presented here clearly substantiates the hypothesis that these two domains are structurally similar. AFPs make extensive hydrogen bonds during ice binding (52), so it may not be surprising that these proteins have a propensity to bind polar sugar molecules. Indeed, our current observations add NeuB to the growing list of AFP homologues that interact with sugars and polysaccharides (type I, Ca^{2+}-dependent lectins; type IV, lipoprotein domain) (52); it represents the first reported case for a type III AFP.

The Active Site of NeuB—To confirm the location of the active site of sialic acid synthase, NeuB crystals were soaked with a large excess of rManNAc and PEP (see "Experimental Procedures"). The reduced ManNAc contains a hydroxyl group as opposed to an aldehyde group at C1, thereby prohibiting the cyclization of the sugar and removing the reactive carbonyl group that would cause the reaction to proceed to completion. Under these conditions, electron density for Mn^{2+}, rManNAc, and PEP was clearly visible at 1σ and 2σ in the $F_o - F_c$ maps (before any additional refinement) and fully occupied within the active site (Fig. 4*a*). Further rounds of refinement improved substrate density visibility.

As with other enzymes that assume a TIM barrel topology, the active site of sialic acid synthase is located in a deep depression at the C-terminal end of the barrel. However, in NeuB, the unique antifreeze-like domain of the second monomer of the homodimer essentially seals off the active site from bulk solvent as well as providing specific residues that come into close contact with the bound substrates. The majority of the residues within the active site come from loop regions and S2 and S4 of the C-terminal end of the TIM barrel, with

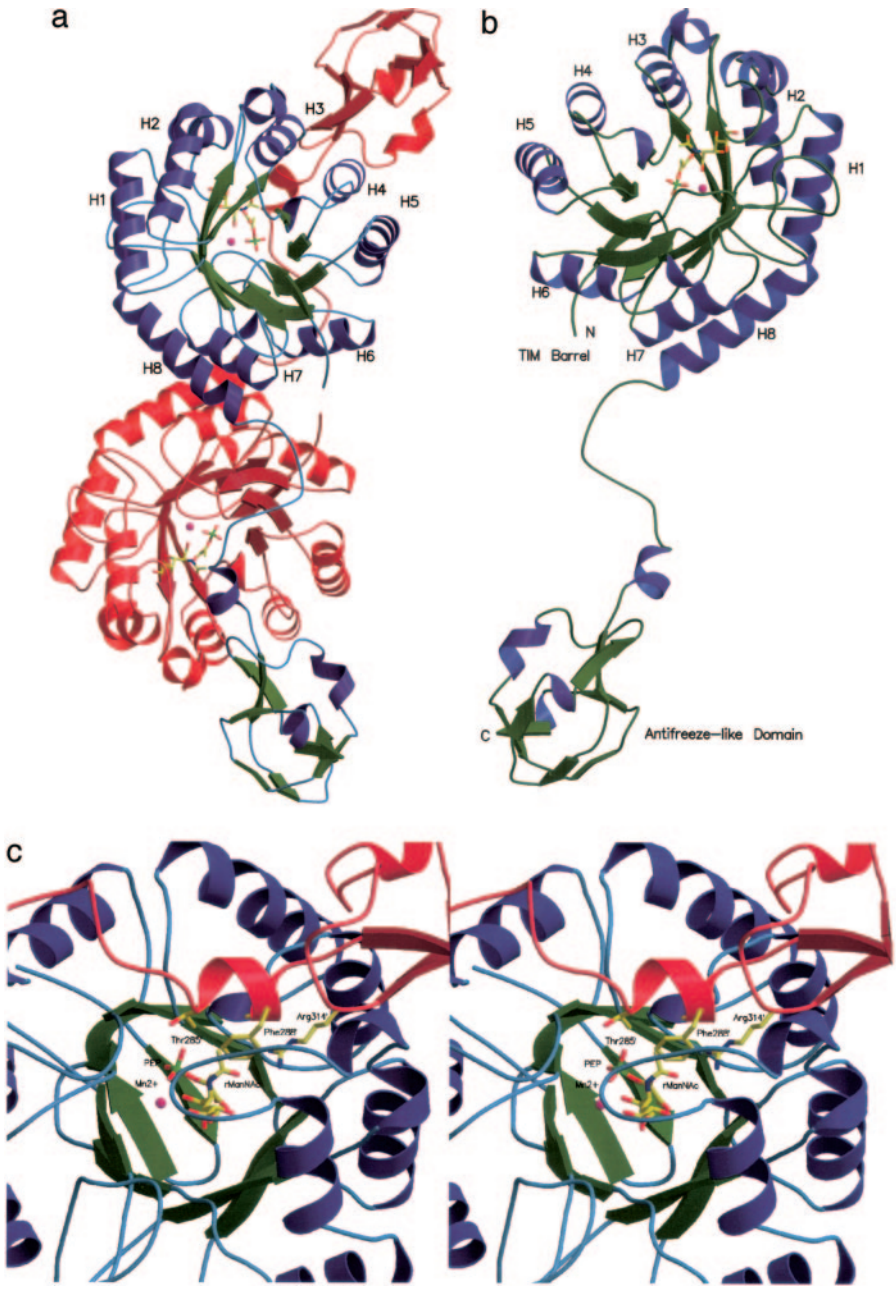

FIG. 3. **Overall architecture of NeuB.** *a*, arrangement of the NeuB domain-swapped homodimer. One monomer is represented in *blue* and *green*, whereas the other monomer is represented in *red* and *orange*. Secondary structure elements are represented as *ribbons*. Helices that are part of the $(\beta/\alpha)_8$ barrel are labeled for the monomer and are represented in *blue* and *green*. Reduced ManNAc and PEP within the active site of NeuB are shown in *stick representation* with carbon atoms in *yellow*, oxygen atoms in *red*, nitrogen atoms in *blue*, phosphorus atoms in *green*, and the metal co-factor Mn^{2+} in *magenta*. *b*, view of the NeuB monomer showing the TIM barrel and antifreeze-like domain with bound reduced ManNAc, PEP, and metal co-factor. The N terminus, C terminus, and individual helices that are part of the TIM barrel are labeled. *c*, stereoview of the antifreeze-like domain and TIM barrel domain interface within the NeuB homodimer. Individual residues (Thr-285′, Phe-288′, and Arg-314′) from the antifreeze-like domain that are positioned within the active site cavity are shown in *stick representation*.

additional contacts made by the helix and coiled region of the linker domain and an extended 11-residue loop of the antifreeze like domain (residues 285–314).

We were prompted to include 10 mM Mn^{2+} in our crystallization conditions by earlier studies which showed that NeuB requires a metal co-factor for activity, with Mn^{2+} having the greatest effect and Co^{2+} having a somewhat lesser effect (11). Our results indicate that the metal co-factor is important for both the structure and catalytic activity of NeuB. It was observed that purified NeuB only formed crystals in the presence of a metal co-factor, with the largest crystals forming in the presence of Mn^{2+}. The metal co-factor is coordinated within the active site in a octahedral manner with His-215 (2.3 Å), His-236 (2.4 Å), O2P from PEP (2.1 Å), and W1 (2.2 Å) forming the equatorial plane and O1 from rManNAc (2.6 Å) and W2 (2.4 Å) filling the axial positions (Fig. 4*b*). The observed direct binding of the hydroxyl group from the sugar substrate suggests that the carbonyl group of non-reduced ManNAc would be in an ideal position to be activated by the metal ion.

The carboxylate and phosphate groups of PEP make several hydrogen bonds with side chains from conserved residues in the active site (Fig. 4*b*). The majority of contacts are made between the *si* face of PEP and the enzyme, with few contacts being made with the *re* face of the substrate. The phosphate group of PEP is tightly anchored by hydrogen bonding to a number of conserved serine residues (Ser-132, -154, -213) and Asn-184. The carboxylate of PEP also forms favorable electrostatic interactions with the side chains of Lys-129 and Lys-53. The two vinylic carbon atoms of PEP do not form interactions with any active site residues because they are coordinated toward the central region of the cavity, thereby making them freely accessible for interactions with the bound sugar substrate.

The majority of mechanisms proposed for the various PEP-utilizing synthases imply that the reactions proceed via an open chain form of the sugar (18–22, 26–29). Structural studies with rManNAc have enabled us to visualize the binding characteristics of the sugar within the active site of NeuB. Several strong hydrogen bonds are formed between active site residues, such as the highly conserved Asp-247, Gln-55, and

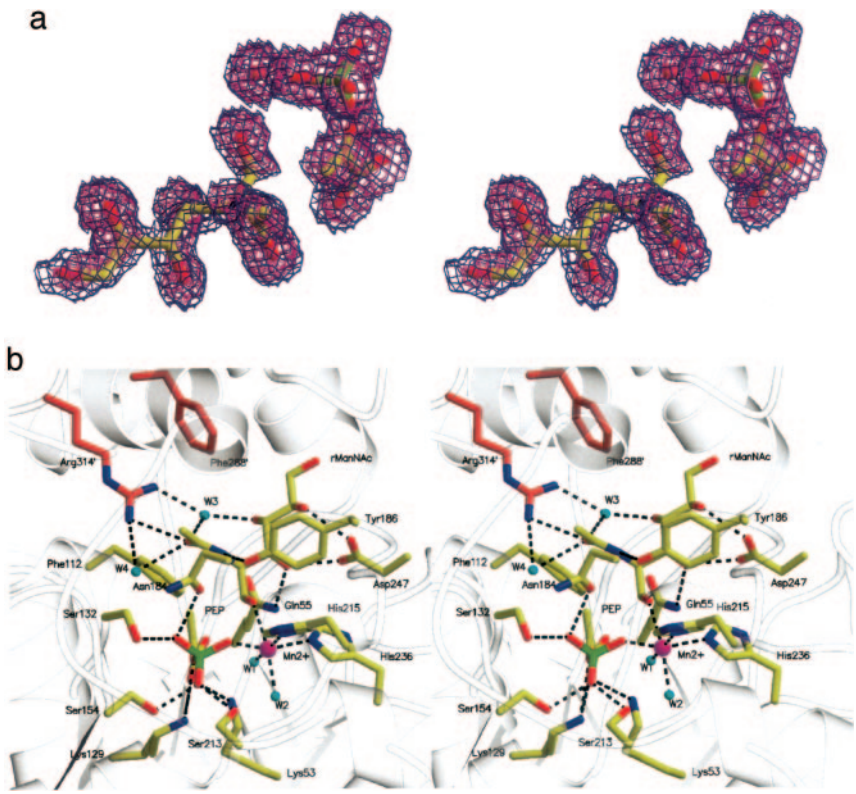

FIG. 4. **The active site of NeuB.** *a*, stereoview of observed electron density of reduced ManNAc, PEP, and Mn^{2+}. Observed density of substrates in initial (before additional refinement) $F_o - F_c$ map contoured at 1σ (blue density) and 2σ. (*magenta*, density). Reduced ManNAc and PEP are represented with carbon atoms in *yellow*, nitrogen atoms in *blue*, oxygen atoms in *red*, and phosphorus atom in *green*. The bound metal co-factor Mn^{2+} is represented in *magenta*. *b*, stereoview of interactions of Mn^{2+}, reduced ManNAc, PEP, and active site residues. Reduced ManNAc and PEP are represented with carbon atoms in *yellow*, nitrogen atoms in *blue*, oxygen atoms in *red*, and phosphorus atom in *green*. Active site residues that interact with bound substrates are also represented in Corey-Pauling-Koltun coloring. Water molecules are *cyan spheres*. The active site residues from the antifreeze-like domain of the interacting monomer are in *red*. *Dotted lines* indicate hydrogen bonds.

Tyr-186, and the functional groups of rManNAc (Fig. 4*b* and 5). In addition, the highly conserved Arg-314′ protrudes from the anti-freeze-like domain of the second monomer to form direct and water-mediated hydrogen bonds with O7 and O4 (acetyl group oxygen) of rManNAc. The conserved side chains of Phe-288′ from the antifreeze-like domain and Phe-112 from the TIM barrel pack against the aliphatic portion of the arginine 314 side chain apparently position the side chain amide optimally for its multiple interactions with bound sugar. The unique main-chain torsional angles associated with the conserved Pro-313 (Fig. 5) directly preceding Arg-314 in the primary sequence of NeuB also plays a role in the correct positioning of its side chain for substrate interactions. The importance of Arg-314 in the catalytic competence of NeuB is indirectly supported by a previous study involving the inhibition of *Streptococcus agalactiae* NeuB through the addition of an arginine-directed modifying reagent, phenylglyoxal (54).

The many favorable non-covalent interactions to the sugar acetyl group, including that from the conserved Arg-314′, is supported by recent work which showed that the catalytic activity of NeuB was optimal with substrates having the physiological acetyl group but was substantially decreased with substrates containing longer acyl side chains (11). The tight packing around the rManNAc we observe in our structure would suggest that the ability to accommodate longer side chains (propanoyl, butanoyl, etc.) would require major conformational adjustments of active site secondary structural elements as well as consequent altered Mn^{2+} and PEP binding, in keeping with the observed loss of activity. DAH7PS and KDO8PS do not process sugar substrates containing acetyl groups, hence, the absence of similar structural interactions in these related proteins. It appears that PEP-utilizing enzymes such KDO8PS, DAH7PS, and NeuB share the same evolutionary background in terms of their TIM barrel protein fold; however, the increasing diversity of reacting substrates likely influenced the formation of novel extensions within groups of these proteins to accommodate the particular features of the substrate, as we observe in the addition of the anti-freeze-like domain for the binding of the *N*-acetyl group in the substrate of NeuB.

Kinetic and Mechanistic Studies on NeuB—To measure the kinetic constants for the NeuB reaction, it was useful to develop a continuous coupled assay. In past research, a stopped thiobarbituric assay for NeuNAc formation was employed (55). The recent availability of commercial sources of NeuNAc lyase, however, permitted the development of a coupled assay that monitors the overall conversion of PEP into pyruvate. In the presence of high levels of NeuNAc lyase, any NeuNAc that is formed will be cleaved to pyruvate and ManNAc. The pyruvate can be detected using lactate dehydrogenase and monitoring the decrease in A_{340} due to the consumption of NADH. This assay was used to obtain the kinetic constants of $k_{cat} = 0.9\ s^{-1}$, K_mPEP = 0.25 mM, and K_mManNAc = 9.4 mM (150 mM Tris-acetic acid (pH 8.3), 1 mM Mn^{2+}). These values agree reasonably well with those previously reported for the wild type enzyme isolated from *N. meningitidis* and assayed under similar conditions (K_mPEP = 0.04 mM and K_mManNAc = 6.3 mM (150 mM Tris-acetic acid (pH 8.3), 5 mM Mn^{2+})) (56).

To probe the mechanism of the synthase reaction, [2-^{18}O]PEP was prepared with a 66% enrichment of a single ^{18}O isotope as determined by mass spectral analysis. The location of the isotope was confirmed to be at the C2 position using ^{31}P NMR spectroscopy. The substitution of an ^{16}O isotope for an ^{18}O isotope at a position that is singly bonded to a phosphorus atom will result in an upfield shift in the corresponding ^{31}P NMR signal (57). This effect can clearly be seen in the spectrum of the starting material that shows two phosphorus signals (Δppm = 0.02) for PEP in a 2:1 ratio (Fig. 6, $t = 0$). Upon the addition of sialic acid synthase the signals corresponding to PEP were gradually replaced by those corresponding to inorganic phosphate (Fig. 6, $t = 60$ min). No such change occurred if the experiment was run in the absence of ManNAc, ruling out the possibility that a phosphatase impurity was responsible for this reaction. Examination of the signals due to inorganic phos-

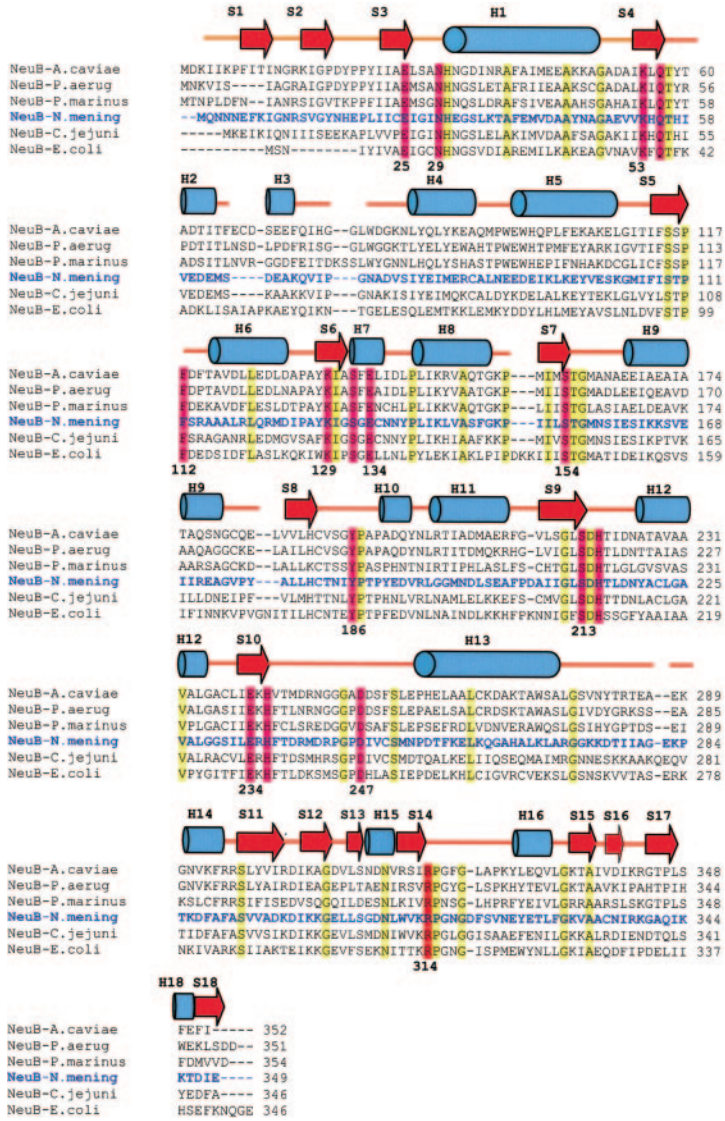

FIG. 5. **Multiple sequence alignment of NeuB orthologues from several bacterial species.** The *N. meningitidis* NeuB sequence is *highlighted* in *blue* and in *bold face*. The secondary structure of *N. meningitidis* NeuB is shown *above* the sequence alignments, with *orange lines* representing coils, *red block arrows* representing strands, and *aquamarine cylinders* representing helices. Conserved active site residues of NeuB within bacterial species are represented in *magenta boxes*. Conserved active site residues of NeuB from the domain swapped partner are represented by *red boxes*. Other conserved residues are indicated with a *yellow* box. The numbering of the *N. meningitidis* sequence is represented bellow the multiple alignment. Sequence alignments were calculated using the program ClustalW (46), and the species sequences are listed in their representative positions in a phylogenetic tree. Sequences from the following species were included (TrEMBL accession codes in parentheses): *Aeromonas caviae* (Q9R9S2), *Pseudomonas aeruginosa* Q8KH52), *Prochlorococcus marinus* (Q7V953), *N. meningitidis* (serogroup B) (Q7DDU0), *C. jejuni* (gene: NeuB1) (Q7BC41), *E. coli* (Q46675).

phate also showed a 2:1 ratio of ^{18}O-labeled to unlabeled compound (Δppm = 0.02), confirming that the label was fully retained in the inorganic phosphate and that the reaction took place via a C—O bond cleavage process (Fig. 2).

Proposed Catalytic Mechanism for Sialic Acid Synthase—Based on our structural and mechanistic observations, one can make several statements relevant to an understanding of the reaction pathway followed by sialic acid synthase. Although the reduced form of ManNAc contains a hydroxyl group instead of an aldehyde at C1, it is presumed that the sugar molecule with the carbonyl group would bind in a similar fashion. At this position, the proximity of the C3 carbon of PEP with C1 of rManNAc is entirely consistent with the observed C—O bond cleavage mechanism in which the initial step involves a C-C bond formation between these groups. The observed vicinity of the rManNAc C-1 hydroxyl and the metal ion (2.5 Å) strongly suggests that the addition is promoted via electrostatic catalysis in which the metal polarizes the carbonyl. Under this scenario the *si* side of PEP would nucleophilically attack the *si* side of ManNAc at the C═O double bond, agreeing with the findings by Sundaram *et al.* (11). The intimate interaction of the carbonyl group with the metal ion and its importance in promoting nucleophilic attack explains the differences in enzyme activity observed with varying divalent metal ion bound in the active site, with Mn^{2+} exhibiting the greatest catalytic influence on the mechanism (11). This observation differs quite notably from recent reports on the metal-dependent KDO8P synthase and DAH7P synthase that state the metal does not play a direct role in catalysis (19–21). Instead, the metal is proposed to be important in maintaining the correct orientation of substrates/amino acids within the active site such that the delivery of water is facilitated. Recent studies have shown that sialic acid synthase condenses the *si* face of PEP with the *si* face of the aldehyde group of ManNAc to form sialic acid (11). The three-dimensional structure of the substrate-bound NeuB is consistent with this conclusion as PEP is bound in such a position that would facilitate the *si* face addition of the substrate to the sugar molecule. C1 and C2 of PEP are positioned toward the center of the cavity where residues from the anti-freeze-like domain are positioned and are twisted (~30°) from planarity with the carboxyl group of the substrate to facilitate the *si* face condensation. This deviation from planarity is unusual; however, it appears to be critical for the mechanism to proceed via nucleophilic addition of C3 of PEP to the sugar substrate. The twist in PEP is also evident to a lesser degree in PEP-bound DAH7P synthase structures (21, 22, 58). The greater degree of deviation from planarity in the bound PEP of NeuB is possibly due to the presence of residues from the anti-freeze like domain. Whereas all the active site residues from DAH7PS come from a single domain, NeuB contains ac-

tive site residues from an alternate domain that is positioned at a slightly different location, requiring a greater twist in the C1 and C2 atoms of PEP.

PEP-utilizing enzymes that promote condensations via a C—O bond cleavage process are expected to catalyze the formation of a tetrahedral intermediate (Fig. 2). This intermediate may be formed in a stepwise fashion in which the addition of PEP to the aldehyde first generates an oxocarbenium ion intermediate, and water subsequently adds to give the tetrahedral adduct (shown in Fig. 2). Alternatively, the water may add in concert with the addition of PEP to give the intermediate in a single step. The strongest support for the oxocarbenium intermediate, or oxocarbenium-like transition state, is found in work on KDO8P synthase in which a cationic mimic of the intermediate has been shown to be a potent inhibitor of enzyme activity (18, 27, 29). In sialic acid synthase, electrostatic stabilization of this intermediate may come from anionic residues such as Glu-25, Glu-134, Glu-234 (Fig. 7). Alternatively, the highly anionic nature of PEP itself may suffice to provide the requisite electrostatic stabilization. In a subsequent step, water is expected to add to the C2 position of the adduct, generating a tetrahedral intermediate.

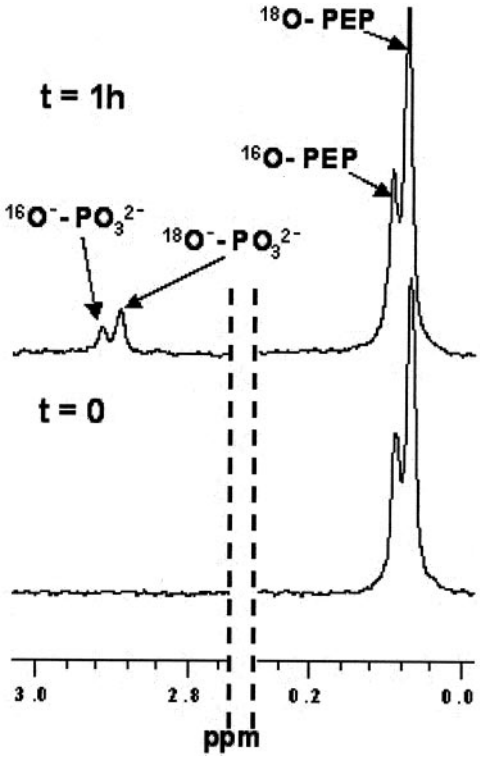

FIG. 6. **^{31}P NMR spectra monitoring the conversion of partially labeled [2-^{18}O]PEP into partially ^{18}O-labeled phosphate by NeuB.** The *lower panel* shows the spectrum before the addition of NeuB. The *upper panel* shows the spectrum taken after 1 h of incubation.

There are two possibilities for this intermediate step. One water molecule, W4 (Fig. 7), sits 3.3 Å away from the *re* face of PEP, and the other, W2, (Fig. 7) sits 3.9 Å away from the *si*-face of PEP. Deprotonation of the water molecule on the *re* face would likely be carried out by the active site base Glu-134. Alternatively, metal-assisted deprotonation of the *si* face water molecule could facilitate hydroxide delivery to the C2 position of PEP. Glu-25 or Glu-234 could potentially act as the catalytic base for the deprotonation step of the *si* face water molecule. Further analysis would be required to determine the exact nature of the formation of the tetrahedral intermediate.

The breakdown of the tetrahedral intermediate with loss of phosphate would likely employ similar catalytic machinery. Ionization of the C2 hydroxyl could be assisted by coordination to the metal or by the involvement of an active site base such as Glu-25, Glu-134, or Glu-234. The resulting open chain form of sialic acid would likely be released into solution where it would spontaneously cyclize to give the pyranose form of the molecule. Alternatively, the enzyme may catalyze the ring opening and ring closing steps of the overall reaction. A final mechanism that involves P—O bond cleavage has been suggested for these enzymes and involves cyclization of the oxocarbenium ion intermediate by attack from the hydroxyl group at C6 (not shown). This directly generates a pyranose form of the tetrahedral intermediate. Water would then replace the phosphate in an S_N1 process involving a cyclic oxocarbenium ion intermediate. The extended conformation of the bound substrates observed in this structure argues against such a mechanism. Furthermore, extensive mechanistic studies on KDO8P synthase eventually ruled out such a mechanism with that enzyme (28).

Conclusion—The importance of understanding the mechanism of sialic acid production is made evident by the vital role this sugar plays in a number of biological processes. Their widespread existence in bacteria enables various pathogens to avert host mammalian host defenses and makes them an attractive target for the development of novel antibiotics. There is also obvious industrial potential for sialic acid synthases in the large scale production of sialic acid containing reagents. We report the first solved crystal structure of a sialic acid synthase complexed with Mn^{2+} and its natural substrate PEP and substrate analog rManNAc. We also demonstrate that the synthase employs a C—O bond cleavage process during catalysis and report a new continuous assay to monitor the reaction kinetics. NeuB exists as a domain-swapped dimer that appears to be mechanistically important for the creation of the NeuB active site because it provides contacts for enzyme-sugar substrate interactions. In addition, the bound metal appears to play a catalytic role in the production of sialic acid, an observation that contrasts against recent enzymatic research on DAH7PS and KDO8PS (19–21). Experiments are currently under way to observe the binding interactions of other substrate analogues and inhibitors with NeuB. The information

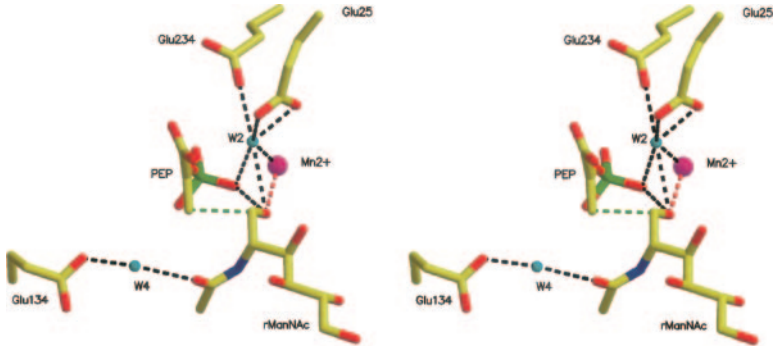

FIG. 7. **Stereoview of proposed catalytic residues involved in the NeuB reaction.** H-bonds are indicated as *black dotted lines*. The covalent bond formed in the condensation reaction between atoms of PEP and ManNAc is indicated with a *green dotted line*. The metal and rManNAc interaction is indicated with a *red dotted line*. Catalytic residues and substrates are represented as *sticks* in Corey-Pauling-Koltun colors. Water molecules are shown as *cyan spheres*, and the metal ion is shown in *magenta*.

gathered from these complexes will further the understanding of the essential process of sialic acid synthesis.

Acknowledgments—We thank Beamline 8.2.1 and 8.2.2 at the Advanced Light Source and the United States Department of Energy for access to the synchrotron radiation used in this study. We thank Dr. Scott Dick for the initial cloning of *neuB* from *N. meningitidis*. We also thank Richard Pfuetzner for assistance with static light scattering and Michela Bertero, Denis Brochu, Cecilia Chiu, Paula Lario, Lodovica Loschi, and Calvin Yip for additional technical assistance.

REFERENCES

1. Varki, A. (1993) *Glycobiology* **3,** 97–130
2. Rosenberg, A. (1995) *Biology of the Sialic Acids*, Plenum Press, New York
3. Finne, J. (1985) *Trends Biochem. Sci.* **10,** 129–132
4. Grossmann, M., Wong, R., Teh, N. G., Tropea, J. E., East-Palmer, J., Weintraub, B. D., and Szkudlinski, M. W. (1997) *Endocrinology* **138,** 92–100
5. Fukuda, M. (1996) *Cancer Res.* **56,** 2237–2244
6. Takano, R., Muchmore, E., and Dennis, J. W. (1994) *Glycobiology* **4,** 665–674
7. Masson, L., and Holbein, B. E. (1983) *J. Bacteriol.* **154,** 728–736
8. Annunziato, P. W., Wright, L. F., Vann, W. F., and Silver, R. P. (1995) *J. Bacteriol.* **177,** 312–319
9. Vann, W. F., Tavarez, J. J., Crowley, J., Vimr, E., and Silver, R. P. (1997) *Glycobiology* **7,** 697–701
10. Linton, D., Karlyshev, A. V., Hitchen, P. G., Morris, H. R., Dell, A., Gregson, N. A., and Wren, B. W. (2000) *Mol. Microbiol.* **35,** 1120–1134
11. Sundaram, A. K., Pitts, L., Muhammad, K., Wu, J., Betenbaugh, M., Woodard, R. W., and Vann, W. F. (2004) *Biochem. J.* **383,** 83–89
12. Comb, D. G., and Roseman, S. (1960) *J. Biol. Chem.* **235,** 2529–2537
13. Roseman, S. (1962) *Proc. Natl. Acad. Sci. U. S. A.* **48,** 437–441
14. Warren, L., and Blacklow, R. S. (1962) *J. Biol. Chem.* **237,** 3527–3534
15. Levin, D. H., and Racker, E. (1959) *J. Biol. Chem.* **234,** 2532–2539
16. DeLeo, A. B., and Sprinson, D. B. (1968) *Biochem. Biophys. Res. Commun.* **32,** 873–877
17. Radaev, S., Dastidar, P., Patel, M., Woodard, R. W., and Gatti, D. L. (2000) *J. Biol. Chem.* **275,** 9476–9484
18. Asojo, O., Friedman, J., Adir, N., Belakhov, V., Shoham, Y., and Baasov, T. (2001) *Biochemistry* **40,** 6326–6334
19. Shulami, S., Furdui, C., Adir, N., Shoham, Y., Anderson, K. S., and Baasov, T. (2004) *J. Biol. Chem.* **279,** 45110–45120
20. Furdui, C., Zhou, L., Woodard, R. W., and Anderson, K. S. (2004) *J. Biol. Chem.* **279,** 45618–45625
21. Shumilin, I. A., Bauerle, R., Wu, J., Woodard, R. W., and Kretsinger, R. H. (2004) *J. Mol. Biol.* **341,** 455–466
22. Konig, V., Pfeil, A., Braus, G. H., and Schneider, T. R. (2004) *J. Mol. Biol.* **337,** 675–690
23. Wagner, T., Shumilin, I. A., Bauerle, R., and Kretsinger, R. H. (2000) *J. Mol. Biol.* **301,** 389–399
24. Banner, D. W., Bloomer, A. C., Petsko, G. A., Phillips, D. C., Pogson, C. I., Wilson, I. A., Corran, P. H., Furth, A. J., Milman, J. D., Offord, R. E., Priddle, J. D., and Waley, S. G. (1975) *Nature* **255,** 609–614
25. Baardsnes, J., and Davies, P. L. (2001) *Trends Biochem. Sci.* **26,** 468–469
26. Howe, D. L., Sundaram, A. K., Wu, J., Gatti, D. L., and Woodard, R. W. (2003) *Biochemistry* **42,** 4843–4854
27. Kaustov, L., Kababya, S., Belakhov, V., Baasov, T., Shoham, Y., and Schmidt, A. (2003) *J. Am. Chem. Soc.* **125,** 4662–4669
28. Liang, P. H., Lewis, J., Anderson, K. S., Kohen, A., D'Souza, F. W., Benenson, Y., and Baasov, T. (1998) *Biochemistry* **37,** 16390–16399
29. Wang, J., Duewel, H. S., Woodard, R. W., and Gatti, D. L. (2001) *Biochemistry* **40,** 15676–15683
30. DeLeo, A. B., Dayan, J., and Sprinson, D. B. (1973) *J. Biol. Chem.* **248,** 2344–2353
31. Hedstrom, L., and Abeles, R. (1988) *Biochem. Biophys. Res. Commun.* **157,** 816–820
32. Seeholzer, S. H., Jaworowski, A., and Rose, I. A. (1991) *Biochemistry* **30,** 727–732
33. Matte, A., Tari, L. W., Goldie, H., and Delbaere, L. T. J. (1997) *J. Biol. Chem.* **272,** 8105–8108
34. Barbosa, J. A. R. G., Smith, B. J., DeGori, R., Ooi, H. C., Marcuccio, S. M., Campi, E. M., Jackson, W. R., Brossmer, R., Sommer, M., and Lawrence, M. C. (2000) *J. Mol. Biol.* **303,** 405–421
35. Ganguli, S., Zapata, G., Wallis, T., Reid, C., Boulnois, G., Vann, W. F., and Roberts, I. S. (1994) *J. Bacteriol.* **176,** 4583–4589
36. Doublie, S. (1997) *Methods Enzymol.* **276,** 523–530
37. Otwinoski, Z., and Minor, W. (1997) *Methods Enzymol.* **276,** 307–326
38. Leslie, A. (1992) *Joint CCP4 + ESF-EAMCB Newsletter on Protein Crystallography*, Vol. 26, Daresbury Laboratory, Warrington, UK
39. Potterton, E., Briggs, P., Turkenburg, M., and Dodson, E. (2003) *Acta Crystallogr. D Biol. Crystallogr.* **59,** 1131–1137
40. Weeks, C. M., and Miller, R. (1999) *J. Appl. Crystallogr.* **32,** 120–124
41. Terwilliger, T. C., and Berendzen, J. (1999) *Acta Crystallogr. D Biol. Crystallogr.* **55,** 849–861
42. La Fortelle, E. D., Irwin, J. J., and Bricogne, G. (1997) *Crystallogr. Comput.* **7,** 1–9
43. Terwilliger, T. C. (2000) *Acta Crystallogr. D Biol. Crystallogr.* **56,** 965–972
44. McRee, D. E. (1999) *J. Struct. Biol.* **125,** 156–165
45. Brunger, A. T., Adams, P. D., Clore, G. M., DeLano, W. L., Gros, P., Grosse-Kunstleve, R. W., Jiang, J. S., Kuszewski, J., Nilges, M., Pannu, N. S., Read, R. J., Rice, L. M., Simonson, T., and Warren, G. L. (1998) *Acta Crystallogr. D Biol. Crystallogr.* **54,** 905–921
46. Laskowski, R. A., MacArthur, M. W., Moss, D. S., and Thornton, J. M. (1993) *J. Appl. Crystallogr.* **26,** 283–291
47. Kraulis, P. (1991) *J. Appl. Crystallogr.* **24,** 946–950
48. Merritt, E. A., and Bacon, D. J. (1997) *Methods Enzymol.* **277,** 505–524
49. Bondinell, W. E., Vnek, J., Knowles, P. F., Sprecher, M., and Sprinson, D. B. (1971) *J. Biol. Chem.* **246,** 6191–6196
50. Vialletelle, V., Rabiller, C., Heisler, A., and Levayer, F. (1992) *Tetrahedron Assymmetry* **3,** 673–676
51. Jia, Z., DeLuca, C. I., Chao, H., and Davies, P. L. (1996) *Nature* **384,** 285–288
52. Davies, P. L., and Sykes, B. D. (1997) *Curr. Opin. Struct. Biol.* **7,** 828–834
53. Hwang, T. S., Hung, C. H., Teo, C. F., Chen, G. T., Chang, L. S., Chen, S. F., Chen, Y. J., and Lin, C. H. (2002) *Biochem. Biophys. Res. Commun.* **295,** 167–173
54. Suryanti, V., Nelson, A., and Berry, A. (2003) *Protein Expression Purif.* **27,** 346–356
55. Warren, L. (1959) *J. Biol. Chem.* **234,** 1971–1975
56. Blacklow, R. S., and Warren, L. (1962) *J. Biol. Chem.* **237,** 3520–3526
57. Cohn, M., and Hu, A. (1978) *Proc. Natl. Acad. Sci. U. S. A.* **75,** 200–203
58. Shumilin, I. A., Bauerle, R., and Kretsinger, R. H. (2003) *Biochemistry* **42,** 3766–3776

Structural and Mechanistic Analysis of Sialic Acid Synthase NeuB from *Neisseria meningitidis* in Complex with Mn^{2+}, Phosphoenolpyruvate, and *N*-Acetylmannosaminitol

Jason Gunawan, Dave Simard, Michel Gilbert, Andrew L. Lovering, Warren W. Wakarchuk, Martin E. Tanner and Natalie C. J. Strynadka

J. Biol. Chem. 2005, 280:3555-3563.
doi: 10.1074/jbc.M411942200 originally published online October 29, 2004